

lines L_x .

Restricting our attention to the physical plane considered by Riedel, it is clear that the crossover lines must approach the TCP along the \bar{x}_3 axis if (3) is *not* an equality. Since the domain in which thermodynamic functions satisfy TCP scaling is only a limited region, and since near the TCP, the position of the crossover lines L_x is close to the \bar{x}_3 direction, the lines L_x are fairly accurately placed. The "metric problem"¹ is thus considerably simplified and may even be effectively disregarded in *nondegenerate* cases.

*The Blume-Emery-Griffiths (BEG) model.*⁷—An example for which the wings' positions are known and for which we can solve for the relative values of \bar{a}_1 , \bar{a}_2 , and \bar{a}_3 is the BEG spin model for He³-He⁴ mixtures, which has been treated extensively by mean-field theory.⁷ We find that for this model, $\bar{a}_1:\bar{a}_2:\bar{a}_3=5:4:2$. Hence, the mean-field-theory solution of the BEG model exemplifies Case I, $\bar{a}_1 > \bar{a}_2 > \bar{a}_3$.

Critical-point exponents in terms of \bar{a}_j .—These may be obtained by appropriate differentiation of Eq. (1). E.g., $\chi \sim (T - T_t)^{-\bar{\gamma}}$ with $-\bar{\gamma} = (1 - 2\bar{a}_2)/\bar{a}_2$, and \bar{a}_2 is determined *uniquely* by $\bar{\gamma}$. A number of "physical-plane exponents" are expressible in terms of \bar{a}_2 , \bar{a}_3 . E.g., for the Ising metamagnet FeCl₂,¹⁰ $\bar{\gamma} \cong \frac{1}{2}$ and $\varphi \equiv \bar{a}_3/\bar{a}_2 \cong \frac{1}{2}$; hence $\bar{a}_2 \cong \frac{2}{3}$, $\bar{a}_3 \cong \frac{1}{3}$. Knowledge of the behavior of M_{st} or χ_{st} will yield \bar{a}_1 .

We wish to thank F. Harbus for useful discussions.

* Portions of this work were presented at the March 1972 meeting of the American Physical Society; see Bull. Amer. Phys. Soc. **17**, 277 (1972). Supported by the Laboratory for Nuclear Science (Massachusetts Institute of Technology), the National Science Foundation, the U. S. Office of Naval Research, the U. S. Office of Scientific Research, and the National Aeronautics and Space Administration.

†Permanent address: Riddick Laboratories, North Carolina State University, Raleigh, N. C. 27607.

¹E. K. Riedel, Phys. Rev. Lett. **28**, 675 (1972).

²R. B. Griffiths, Phys. Rev. Lett. **24**, 715 (1970).

³R. B. Griffiths and J. C. Wheeler, Phys. Rev. A **2**, 1047 (1970).

⁴The reader may have some difficulty at this point in making correspondence between the present notation and that of Ref. 1. There is no counterpart to \bar{x}_1 because the equations of Ref. 1 were restricted to $\bar{x}_1 = 0$. The variables \bar{x}_2, \bar{x}_3 are denoted by μ_1, μ_2 , respectively, in Ref. 1.

⁵For a systematic application of generalized homogeneous functions to scaling, see A. Hankey and H. E. Stanley, Phys. Rev. B (to be published).

⁶For example, $\varphi \equiv \bar{a}_3/\bar{a}_2$, $-\bar{\gamma} = (1 - 2\bar{a}_2)/\bar{a}_2$, $-\bar{\gamma}_{st} = (1 - 2\bar{a}_1)/\bar{a}_2$, $\bar{\beta}_{st} = (1 - \bar{a}_1)/\bar{a}_2$.

⁷M. Blume, V. J. Emery, and R. B. Griffiths, Phys. Rev. A **4**, 1071 (1971).

⁸There is one exceptional case which is not treated here.

⁹In the event that one finds a model system displaying this behavior, then one must test the possibility that two scaling powers are equal (Ref. 6); otherwise the scaling hypothesis (1) is *invalid* for this model.

¹⁰F. Harbus, private communication. See also F. Harbus and H. E. Stanley, Phys. Rev. Lett. **29**, 58 (1972).

Q-Switch and Polarization Domains in Antiferromagnetic Chromium Observed with Neutron-Diffraction Topography

Masami Ando and Sukeaki Hosoya

Institute for Solid State Physics, University of Tokyo, Roppongi, Minato-ku, Tokyo, Japan

(Received 17 March 1972)

The Q-switch and polarization domain configurations in a nearly perfect Cr single crystal has been directly observed by neutron-diffraction topography in the AF₁ and AF₂ phases. The size of the domains proves to be as large as 10⁻³ to 10⁻² cm³ in either phase. As far as the present observation is concerned, each domain in the AF₂ phase splits into domains in the AF₁ phase, with two possible polarizations of the transverse spin-density wave.

In a previous paper¹ it was reported that the Q-switch domain boundaries in antiferromagnetic Cr in the AF₂ phase at 78 K were observed by means of x-ray double-crystal topography, using the slight deviation from cubic symmetry. In the present paper, unambiguous direct observations

are reported on Q-switch and polarization domains by the use of new neutron topography. As is well known, there can be three kinds of domains in the AF₂ phase and six in the AF₁, and each of them gives independent neutron satellite diffractions at different positions in the recipro-

cal space. Therefore, it is obvious that the neutron-diffraction topograph for each domain can be taken by using each relevant satellite reflection, provided the domain size is larger than the resolution. This has been successfully carried out.

The Cr crystal, with its $[001]$ axis parallel to the goniometer axis of a usual neutron spectrometer, was held in vacuum in the cryostat² and cooled through a copper block on which a heater was wound. Neutron topographs were taken by a neutron Polaroid camera,³ by using a monochromatic neutron beam⁴ with a wavelength of about 1.22 \AA from the 10-MW JRR-2 reactor of the Japan Atomic Energy Research Institute. It was not necessary for the Cr sample to be traversed because its whole area was observed at a time by a wide and divergent neutron beam from a Ge monochromator. The sample-film distance was about 230 mm, which was much longer than in the usual case of x-ray-diffraction topography. However, the present method is analogous to the transmission Berg-Barrett method⁵⁻⁷ in terms of x-ray topography. The flux density at the specimen was about $4.5 \times 10^4 \text{ neutrons cm}^{-2} \text{ sec}^{-1}$. Exposure time necessary for taking each magnetic domain was about 70–120 min, although high-speed Polaroid films of type 47 (ASA 3000) were used. All topographs were taken so that the diffracted beam would fall upon a fluorescent screen perpendicularly.

The resolution of the present topography is limited almost equally by both the geometrical ar-

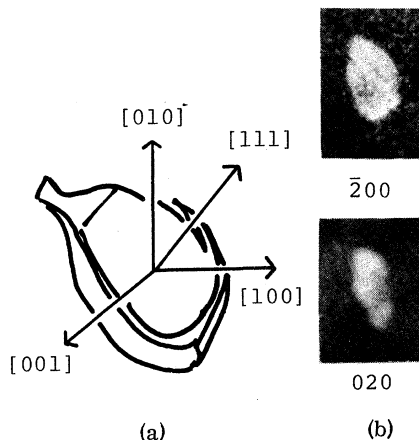


FIG. 1. (a) Perspective view of the Cr specimen; the plane of incidence is near the (001) plane and the largest face is (111) as shown. (b) Cr topographs taken by nuclear scattering $\bar{2}00$ and 020 . These correspond to the x-ray topographs in a previous paper (Ref. 1). The white parts correspond to the regions upon which more neutrons fell. Magnification, 1.7.

range of the apparatus and the grain size of the $\text{Li}^6\text{F-ZnS}$ fluorescent screen employed. If the specimen includes many different domains smaller than the present resolution, every topograph taken with each satellite reflection should always show the whole area of a crystal with different intensity, depending upon the existing ratio of the relevant domain. However, the domain size proved to be large enough to be observed even by a neutron Polaroid camera as shown in the following. Incidentally, the Gd-Rh foil technique,⁸ with far better resolution, proved impractical for the available neutron flux and machine time, because, in fact, it required over 1 week to take one topograph with a satellite reflection.

The sample was a nearly perfect single crystal⁹ having as-grown faces $\{111\}$; the largest face will be referred to as (111) , as shown in Fig. 1(a). In previous x-ray work, this (111) face of the same sample was used to obtain 211 reflection topographs by the $(+, -)$ double-crystal parallel setting. Figure 1(b) shows neutron topographs of this sample taken with nuclear scattering, $\bar{2}00$ and 020 reflections. These topographs indicate the front and side views of the whole sample, re-

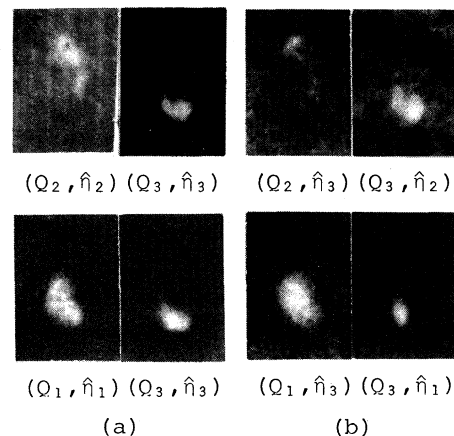


FIG. 2. Cr domain topographs taken by magnetic satellite scattering. The notation under the topographs refers to each satellite shown in Fig. 4. The topographs in the upper and lower rows were taken with satellite reflections near $\bar{1}00$ and 010 , respectively. (a) Taken at 81 K (AF_2 phase); (b) at 140 K (AF_1 phase). (a) shows all domains of the three kinds in the AF_2 phase; (b) shows four out of a possible six domains. (b) clearly shows that the (Q_2, \hat{h}_2) domain is only a small part of the (Q_2, \hat{h}_2) domain and that, on the other hand, the (Q_1, \hat{h}_3) domain has almost the same area as the (Q_1, \hat{h}_1) domain. It also shows that the (Q_3, \hat{h}_3) domain in the AF_2 phase has split into (Q_3, \hat{h}_2) and (Q_3, \hat{h}_1) domains in the AF_1 phase, although the former seems to be subject to noise.

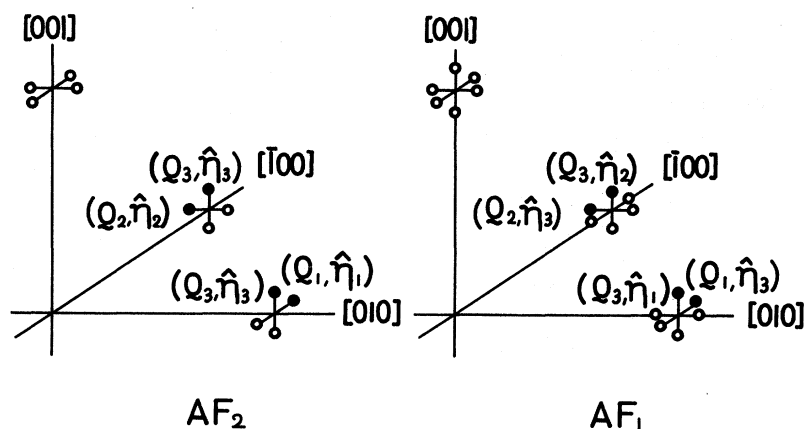


FIG. 3. Schematic of the reciprocal lattice showing magnetic-satellite-scattering positions of a Cr single crystal. AF_2 and AF_1 phases correspond to longitudinally and transversely polarized SDW, respectively. Solid circles indicate reflections used in the present observation. Each was selected out of the two equivalent reflections so that the larger projection could be obtained. (Q_2, \hat{n}_1) and (Q_1, \hat{n}_2) domains in the AF_1 phase could not be observed since the $[001]$ crystal axis parallel to the goniometer axis could not be rotated by 90° around either the $[100]$ or $[010]$ axis.

spectively. For convenience, the same Miller indices as used in the previous note¹ are followed in the present paper. The diffraction geometry was chosen so that the $\bar{2}00$ topograph and satellite topographs near $\bar{1}00$ may have, to a certain extent, a projection similar to the previous x-ray topographs.

Figures 2(a) and 2(b) show neutron topographs of magnetic domains of the same sample taken by neutron beams diffracted from longitudinal and transverse spin-density waves (LSDW and TSDW), respectively. Each white part in the topographs, no doubt, shows a domain which includes only one SDW, because the size and area of the domain topograph did not change even if the crystal was rotated back and forth in an angular range wider than the full-width at half-maximum intensity of the satellite reflection.

In the following, magnetic domains will be specified by (Q_i, \hat{n}_j) ,^{10,11} where Q_i is the propagation vector of SDW's in the direction i , and \hat{n}_j is the unit vector along the spin-polarization direction j ; i and j are 1, 2, or 3, which correspond to the directions $[\pm 100]$, $[0 \pm 10]$, or $[00 \pm 1]$ in the cubic phase, respectively. The positions of magnetic satellite reflections near $\bar{1}00$ and 010 arising from these SDW's are expressed in reciprocal space as in Fig. 3. The topographs in Fig. 2(a) were taken at 81 K in the AF_2 phase, while those in Fig. 2(b) were taken at 140 K in the AF_1 phase. Figure 2(a) clearly shows that each topograph is only a part of the $\bar{2}00$ or 020 topograph, and that the Cr sample used in the present work is composed of only a few magnetic domains. By rais-

ing the temperature of the sample through the spin-flip temperature 122 K, each domain (Q_i, \hat{n}_j) transforms into domains $(Q_i, \hat{n}_j)_{i \neq j}$, as reported in other papers.^{10,11} In the present experiment, only the splitting of the (Q_3, \hat{n}_3) domain could be observed in Fig. 2(b) because of the limitation in diffraction geometry as understood from Fig. 3.

The domains are three-dimensional entities, and the projected shape and area of each domain more or less depend upon the diffraction geometry for taking each topograph due to the relevant satellite reflection. Therefore, overlapping may well occur sometimes among the domains, apart from some penumbras due to angular and wavelength divergences of the beam. The overlapping of areas between the (Q_3, \hat{n}_3) and (Q_1, \hat{n}_1) domains in Fig. 2(a) may thus be interpreted. Note that it is highly improbable that the overlapped area alone includes many domains smaller than the resolution. Therefore, it becomes almost possible to construct the domain configuration in the present Cr sample from Figs. 2(a) and 2(b), as shown in Fig. 4(a).

Figure 4(b) includes the video x-ray topograph (at 114 K)¹² and neutron satellite topographs (at 78 K) of Q -switch domains. Both of these x-ray and neutron topographs were taken after the sample was kept at room temperature, 291–298 K (below the Néel temperature 311 K), for several months and then cooled again to the AF_2 phase. A comparison between two pairs of topographs, (Q_2, \hat{n}_2) and (Q_1, \hat{n}_1) in Figs. 2(a) and 4(b), implies that the Q -switch boundaries may slightly shift, as was observed in the x-ray case, once the sam-

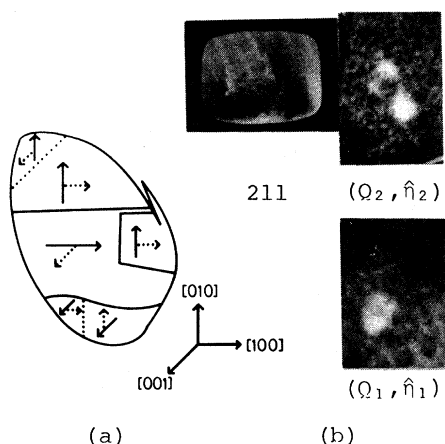


FIG. 4. (a) Sketch of domain distribution obtained from Figs. 2(a) and 2(b); solid and dotted lines, Q -switch and polarization boundaries, respectively. Solid and dotted arrows, propagation vector Q_i and polarization vector \hat{n}_i , respectively. (b) Video x-ray topograph using 211 reflection and neutron satellite topographs in the AF_2 phase, taken about 100 days earlier than Figs. 1(b) and 2 were. Neutron topographs were taken under the same conditions as the (Q_2, \hat{n}_2) and (Q_1, \hat{n}_1) topographs in Fig. 2(a).

ple is kept near the Néel temperature, although a more decisive conclusion warrants further observations.

In sharp contrast to the present observation, the values of the domain size, so far indirectly estimated, have been very small: The values based on a thermal-activation model are $5.3 \times 10^{-16} \text{ cm}^3$ ¹³ (calculated by Werner, Arrott, and Kendrick¹⁰ at 293 K), and $(2.8-4.4) \times 10^{-16} \text{ cm}^3$ (calculated by Steinitz *et al.*¹⁴ at 129 K); the value based on the elasticity data is $1.4 \times 10^{-15} \text{ cm}^3$ (calculated by Munday and Street¹⁵ at 200 K). The present results seem to conflict with the thermal-activation model, but it might be possible to avoid this conflict by an interpretation that a Boltzmann distribution of many small domains, weighted by internal strain fields in favor of one polarization, produced each of the observed large domains. However, this interpretation may not be probable, because the larger domain is found in the more perfect region according to the facts so far observed.

Several conclusions can be drawn from the present work together with the previous work¹: (1) The present direct observation reveals that the domain is as large as 10^{-3} – 10^{-2} cm^3 , at least in a highly perfect single crystal, in contrast to the very small values so far estimated. (2) In

neutron topographs, apart from the poor resolution, the shape of the domain boundaries cannot usually be known, because only the projection is recorded. However, from x-ray topographs, especially reported in the previous work,¹ it can be claimed that the domain configuration should be determined mainly by the strain field so that the strain energy may be relaxed. (3) When a Cr sample undergoes a phase transition from the AF_2 to the AF_1 phase, a Q -switch domain does not split into many small polarization domains, but into a few domains, while the latter domains are not necessarily comparable in size; for example, the domain (Q_1, \hat{n}_3) in Fig. 2(b) is nearly as large as the (Q_1, \hat{n}_1) domain¹⁶ in Fig. 2(a).

The authors are much indebted to Professor A. Arrott for his invaluable discussion on the present results and for his critical reading of the manuscript. They also wish to express their gratitude to Mr. K. Namikawa and Mr. T. Fukamachi for their help in a part of the present work, and to Professor S. Hoshino, Dr. H. Motegi, and Dr. Y. Fujii for the loan of their cryostat.

¹S. Hosoya and M. Ando, Phys. Rev. Lett. **26**, 321 (1971).

²K. Shimaoka, N. Niimura, and S. Hoshino, Jap. J. Appl. Phys. **10**, 933 (1971).

³S. P. Wang, C. G. Shull, and W. C. Phillips, Rev. Sci. Instrum. **33**, 126 (1962).

⁴The neutron beam was obtained by the 311 reflection from Ge, where the scattering angle was 42° . The second-order contamination is negligible since the scattering factor for 622 in Ge is zero. The wavelength dispersion $\Delta\lambda/\lambda$ of the beam is about 2×10^{-3} .

⁵W. F. Berg, Naturwissenschaften **19**, 391 (1931).

⁶W. F. Berg, Z. Kristallogr. **89**, 286 (1934).

⁷C. S. Barrett, Trans. AIME **161**, 15 (1945).

⁸H. Berger, Rev. Sci. Instrum. **33**, 844 (1962).

⁹The Cr crystal was the same single crystal that was used in Ref. 1. The measured value for the full-width at half-maximum intensity of the x-ray 211 reflection was nearly equal to the intrinsic value calculated for a perfect Cr crystal.

¹⁰S. A. Werner, A. Arrott, and H. Kendrick, Phys. Rev. **155**, 528 (1967).

¹¹R. Street, B. C. Munday, B. Window, and I. R. Williams, J. Appl. Phys. **39**, 1050 (1968).

¹²The topograph was taken by an x-ray vidicon camera with PbO target [see J. Chikawa and I. Fujimoto, Appl. Phys. Lett. **13**, 387 (1968)] at the Broadcasting Science Research Laboratories of Nippon Hosokyo. At that time, the sample was cooled by sprayed liquid nitrogen. The results of this experiment were presented at the Spring Meeting of the Physical Society of Japan in 1971 (unpublished) by the present authors together with

J. Chikawa and I. Fujimoto.

¹³This value was recalculated. The value in Ref. 10 seems to be erroneous.

¹⁴M. O. Steinitz, E. Fawcett, C. E. Burleson, J. A. Schaefer, L. O. Frishman, and J. A. Marcus, Phys. Rev. B **5**, 3675 (1972).

¹⁵B. C. Munday and R. Street, J. Phys. F: Proc. Phys.

Soc., London **1**, 498 (1971).

¹⁶In the intensity measurement, at least one case has been reported on the single-Q single-polarization state due to the lack of one polarization in the AF₁ phase. See A. Arrott and S. A. Werner, in *Metallurgical Society Conferences* (Gordon and Breach, New York, 1968), Vol. 43, p. 50.

Theory of Magnetic Fluctuations in Itinerant Ferromagnets*

K. K. Murata and S. Doniach

*Department of Applied Physics, W. W. Hansen Laboratories of Physics,
Stanford University, Stanford, California 94305*

(Received 15 May 1972)

The statistical mechanics of a classical field theory describing mode-mode interactions is shown to lead to a theory of the Curie law and specific-heat anomaly observed in the weak itinerant ferromagnet Sc₃In.

A basic problem in the theory of itinerant ferromagnets is the explanation of the well-defined Curie-law behavior observed in a wide variety of metallic magnets. For strong ferromagnets, such as iron, it seems likely that the formation of local moments above the Curie temperature T_c is responsible, as discussed theoretically by Wang, Evenson, and Schrieffer.¹ For weak ferromagnets with a T_c of a few degrees Kelvin, however, the existence of small saturation moments at $T=0$ of a few percent of a Bohr magneton per formula unit conflicts with this picture, and an alternative description is needed.

In this Letter we give a model field-theory description of the thermodynamic (time-averaged) magnetization fluctuations in an itinerant ferromagnet, and use classical statistical mechanics to relate the observed properties (magnetization, susceptibility, and specific heat) in the transition region to those at $T=0$. Using this approach we are able to give a good account of the observed Curie-law behavior in the weak itinerant ferromagnet Sc₃In, and also to derive a theory of the specific heat in the region of T_c which fits qualitatively the observed specific heat in this material.

The main physical assumption made in the model, which is expressed as an energy functional

$$\mathcal{F} = \int d^3x \left\{ \mu^2 [\nabla m(x)]^2 + \alpha m(x)^2 + \frac{1}{2} \beta m(x)^4 \right\} \quad (1)$$

[where $m(x)$ is a scalar field representing the local order parameter²], is that the parameters μ , α , and β can be treated as approximately temperature independent from $T=0$ up to the region of the Curie temperature for a weak itinerant fer-

romagnet.

On forming the classical free energy^{3,4}

$$F = -k_B T \ln \int \mathcal{D}m e^{-\mathcal{F}/k_B T}, \quad (2)$$

one then finds that the transition is driven by the mode-mode coupling term $\frac{1}{2}\beta m^4$ in Eq. (1). This mechanism for destroying the ordered state is quite different from the mechanism appearing in the Ginzburg-Landau approach to the theory of the superconducting transition.⁵ In the latter case α varies as $T - T_c$ and, as the fluctuations are limited to wavelengths longer than the temperature-dependent inverse coherence length, it is the mode-softening effect which determines the transition.

Using the present assumption of temperature-independent parameters in Eq. (1), we may relate them to properties of the ground-state energy of the interacting electron gas

$$\begin{aligned} \alpha &= \frac{1}{2} \delta^2 E_G / \delta m_{q=0}^2 = \chi_{q=0}^{-1}, \\ \mu^2 &= \frac{1}{2} (d\chi_q^{-1}/dq^2)_{q=0}, \\ \beta &= \frac{1}{6} \delta^4 E_G / \delta m_{q=0}^4, \end{aligned} \quad (3)$$

where χ_q is the generalized susceptibility at $T=0$. Here we are implicitly neglecting nonlocal effects (q dependence) in the m^4 term. Using Eq. (3), the parameters may then be related to the effective band-structure density of states and electron-electron interaction of the Stoner-Wohlfarth theory⁶ by calculating $E_G(m)$ using the Hartree-Fock approximation. One then finds

$$\begin{aligned} \alpha &= N(0)^{-1} [1 - U_{\text{eff}} N(0)], \\ \beta &\propto -N(0)^{-1} N''(0)/N(0)^3. \end{aligned} \quad (4)$$

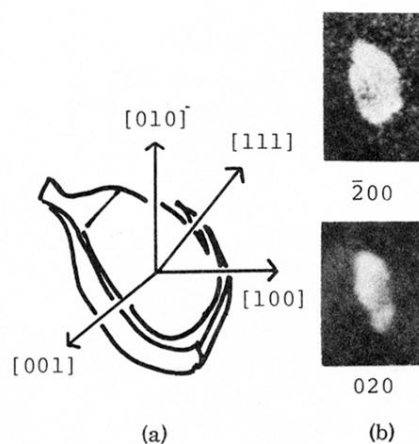


FIG. 1. (a) Perspective view of the Cr specimen; the plane of incidence is near the (001) plane and the largest face is (111) as shown. (b) Cr topographs taken by nuclear scattering $\bar{2}00$ and 020 . These correspond to the x-ray topographs in a previous paper (Ref. 1). The white parts correspond to the regions upon which more neutrons fell. Magnification, 1.7.

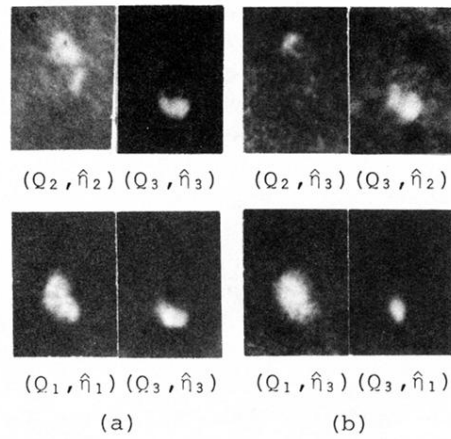


FIG. 2. Cr domain topographs taken by magnetic satellite scattering. The notation under the topographs refers to each satellite shown in Fig. 4. The topographs in the upper and lower rows were taken with satellite reflections near $\bar{1}00$ and 010 , respectively. (a) Taken at 81 K (AF_2 phase); (b) at 140 K (AF_1 phase). (a) shows all domains of the three kinds in the AF_2 phase; (b) shows four out of a possible six domains. (b) clearly shows that the $(Q_2, \hat{\eta}_3)$ domain is only a small part of the $(Q_2, \hat{\eta}_2)$ domain and that, on the other hand, the $(Q_1, \hat{\eta}_3)$ domain has almost the same area as the $(Q_1, \hat{\eta}_1)$ domain. It also shows that the $(Q_3, \hat{\eta}_3)$ domain in the AF_2 phase has split into $(Q_3, \hat{\eta}_2)$ and $(Q_3, \hat{\eta}_1)$ domains in the AF_1 phase, although the former seems to be subject to noise.

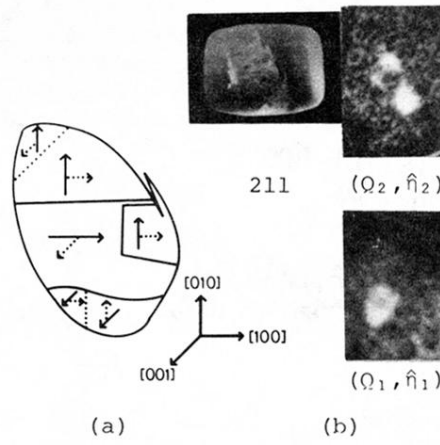


FIG. 4. (a) Sketch of domain distribution obtained from Figs. 2(a) and 2(b); solid and dotted lines, Q -switch and polarization boundaries, respectively. Solid and dotted arrows, propagation vector Q_i and polarization vector \hat{n}_i , respectively. (b) Video x-ray topograph using 211 reflection and neutron satellite topographs in the AF_2 phase, taken about 100 days earlier than Figs. 1(b) and 2 were. Neutron topographs were taken under the same conditions as the (Q_2, \hat{n}_2) and (Q_1, \hat{n}_1) topographs in Fig. 2(a).